



## CFD method for the relationship between the radius size of impellers and cross-sectional average velocity of flow in an oxidation ditch

Jiahao Wei\*, Zhiqiang Xu

State Key Laboratory Base of Eco-Hydraulic Engineering in Arid Area (SKLEHE), Xi'an University of Technology, Xi'an, Shaanxi 710048, China, Tel. +86 18629352022; email: Jwei1995@126.com (J. Wei), Tel. +86 18991169969; email: ZQX1969@126.com (Z. Xu)

Received 15 September 2017; Accepted 9 July 2018

---

### ABSTRACT

This paper is concerned with a numerical simulation method for the influence of radius size of impellers on the cross-sectional average velocity of flow in an oxidation ditch (OD). The velocity and pressure fields are obtained by solving the three-dimensional time-averaged Navier–Stokes equations with renormalized group  $k$ - $\epsilon$  turbulence model using Fluent 6.3.26. Dimensional analysis method is applied to the variables of fluid-flow situation in the OD to find a set of  $\pi$  parameters, by which the relation between the radius size of impellers and the cross-sectional average velocity of the flow was obtained. According to the dimensional analysis and simulation results, the equation for the cross-sectional average velocity of flow varying with the radius size of impellers in the OD was obtained, which can provide a reference in the optimization of designing ODs. At last, the energy efficiency for each impeller at a fixed flow speed and the impeller rotation speed to achieve a reference sectional velocity of 0.3 m/s were analyzed.

*Keywords:* Oxidation ditch; Radius size of impellers; Dimensional analysis; Cross-sectional average velocity of flow; CFD

---

### 1. Introduction

Oxidation ditch (OD) process is one of the most important technologies for wastewater treatment and has been widely used due to its reliability, simplicity of operation, and low-sludge production [1,2], because the flow-field structure in OD has an important influence on its operation efficiency. Therefore, many scholars have carried out a large number of experimental studies and numerical simulation to understand the hydrodynamics of the ditch for its successful design.

Diamantis et al. [3] obtained a conclusion through experimental method that the aeration rate and the distribution of aerators enhance the flow stratification in a full-scale OD. Fan et al. [4] did an experiment on hydraulics in Carousel OD model with one inverted umbrella surface aerator. The analysis of the liquid velocity, particle settling velocity, and solid distribution shows that the flow velocity is higher near

the surface aerator, and the solid content increases gradually away from the surface aerator. Simon [5] investigated the liquid velocity and the power dissipation of unit volume liquid in an OD. Xu et al. [6] studied the longitudinal, transverse, and vertical velocity distributions of a Carousel OD using a particle image velocimetry technology. Fan et al. [7] measured the flow fields in an experimental Carousel OD with two surface aerators like an inverse umbrella with particle dynamic analyzer. It was observed that there was negligible difference between the flow velocities of solid and liquid phases, while the settling velocity of solid was a bit larger than that of liquid due to inertial effect. Liu and He [8] used acoustic Doppler velocimeter (ADV) to analyze the flow fields of ODs under the running of submerged impeller. The results indicated that when the submerged impeller was installed at the middle of water depth, the cross sectional mean velocity was 18% higher than that installed at the bottom, and the power utility rate was also higher, thus the flow

---

\* Corresponding author.

can be much enhanced. Zhao et al. [9] measured the hydraulic characteristics of mixture in an OD, which shows that the flow-field structures of mixture appear a higher similarity under different rotating conditions.

Besides the experimental studies [1–9], computational fluid dynamics (CFD) method is also widely used to OD flow characteristics. Wei et al. [10] performed an experimental and simulation study of hydraulic characteristics in a pilot Carrousel OD for the optimization of submerged depth ratio of surface aerators. The simulation was carried out by large eddy simulation with Smagorinsky model, and the velocity was monitored in the ditches with an ADV method. The best submerged depth ratio of 2/3 for surface aerators was obtained. Liu et al. [11] studied the relationship between the size of impeller radius and the structure of flow field in an OD using the two-phase gas–liquid model and the three-dimensional (3D) realizable  $k$ - $\varepsilon$  turbulence model. The research results show that the ratio 0.218 of the impeller radius to the diameter of the OD channel bend can make the percentage of the fluid with velocity greater than 0.3 m/s to the entire fluid to be greatest, and the length of the backflow region in straight channels to be relatively shorter. The ratio of impeller radius to the diameter of OD channel bend with a value of 0.218 is called the optimal impeller radius ratio. Luo et al. [12] calculated flow fields and hydraulic characteristics of Carrousel OD using  $k$ - $\varepsilon$  turbulence mathematical model and found that the curved channel and vertical plate resistance is the main factor causing the water head loss in Carrousel OD. Yang et al. [13] used FLUENT software to simulate the velocity distribution of the curved channel in an OD, and the result shows that the influence of the shape and position of the guide wall of OD influence flow fields greatly. Wei et al. [14] used the CFD method to simulate the effect of guiding baffles downstream from surface aerators on the flow fields in an OD. Comparisons of the velocity distributions under the two conditions (with and without guiding baffles) show that the installed guiding baffles downstream from the surface aerators can increase the velocity at the ditch bottom, and the vertical velocity distributions in the OD become more uniform, which will help to prevent sludge deposit at the bottom of the OD and have an obvious effect on time prolongation for liquid–gas mixture. Li and Ni [15] simulate the hydrodynamics, oxygen mass transfer, carbon oxidation, nitrification, and denitrification processes in OD using a 3D three-phase fluid model which can provide detailed phase information on the liquid flow field, gas hold-up distribution, and sludge sedimentation. Guo et al. [16] simulated the flow velocity and dissolved oxygen (DO) concentration in the outer channel of an Orbal OD system in a wastewater treatment plant under actual operation conditions, which shows that the flow velocity was heterogeneous in the outer channel, and the DO was also heterogeneously distributed in the outer channel, with concentration gradients occurring along the flow direction as well as in the cross section. This heterogeneous DO distribution created many anoxic and aerobic zones, which may have facilitated simultaneous nitrification–denitrification in the channel.

Wei et al. [17] studied the effect of the submergence depth of impellers on the structure of flow fields in an OD using an experimentally validated numerical tool, based on CFD model, and obtained the optimal submergence depth ratio of 0.45, by which the efficiency of an OD wastewater treatment system will be better improved.

The above references [1–17] mainly study the physical properties of a single-phase or two-phase flow in OD, but do not deal with the influence of the radius size of impellers on the cross-sectional average velocity of flows. With a constant rotational speed, the radius size of impellers has an important influence on the flow velocity distribution and flow structure in OD. When the rotational speed of impellers is fixed at a constant, the larger the radius of impellers, the greater is the average velocity over a cross section. Thus, an appropriate radius for impellers should be proposed for OD to obtain the ideal flow so that the efficiency of water treatment will be increased greatly. Therefore, the objective of this work is to find the variation of average velocity over a cross section with the radius size of impellers by the dimensional analysis method and the solution of 3D time-averaged Navier–Stokes (N–S) equations along with a renormalized group (RNG)  $k$ - $\varepsilon$  turbulence model, which can provide a reference in the designing of ODs.

## 2. Dimensional analysis

The variation of cross-sectional average velocity of flow with radius size of impellers was analyzed by dimensional analysis method. After analysis, we know that the fluid-flow situation depends on the rotational speed  $\omega$  of impellers, the average velocity  $V$  over a cross section, the density  $\rho$  of water, the viscosity  $\nu$  of water, the gravity acceleration  $g$ , several linear dimensions, such as the width  $B$  of the straight channel, the water depth  $H$ , the radius  $r$  of impellers, and the radius  $R_1$  of small bends. Apply dimensional analysis to these variables to find a set of  $\pi$  parameters.

The formula for the fluid-flow situation can be written as follows:

$$V = f(r, \rho, g, \nu, B, H, \omega, R_1) \quad (1)$$

in which there are nine variables, including one dependent variable  $V$  and eight independent variables  $\omega$ ,  $\rho$ ,  $g$ ,  $\nu$ ,  $B$ ,  $H$ ,  $r$ , and  $R_1$ .

As three dimensions are involved, three repeating variables are selected. For complex situations,  $r$ ,  $\rho$ , and  $g$  are generally helpful. There are nine  $\pi$  parameters, so the formula for the relationship between the nine dimensionless numbers ( $\pi$ ) can be expressed as follows [18]:

$$\pi = f(\pi_1, \pi_2, \pi_3, \pi_4, \pi_5, \pi_6, \pi_7, \pi_8) \quad (2)$$

where:

$$\begin{aligned} \pi &= \frac{V}{r^{x_0} \rho^{y_0} g^{z_0}}, \quad \pi_1 = \pi_2 = \pi_3 = 1 \\ \pi_4 &= \frac{\nu}{r^{x_4} \rho^{y_4} g^{z_4}}, \quad \pi_5 = \frac{B}{r^{x_5} \rho^{y_5} g^{z_5}} \\ \pi_6 &= \frac{H}{r^{x_6} \rho^{y_6} g^{z_6}}, \quad \pi_7 = \frac{\omega}{r^{x_7} \rho^{y_7} g^{z_7}} \\ \pi_8 &= \frac{R_1}{r^{x_8} \rho^{y_8} g^{z_8}} \end{aligned} \quad (3)$$

The  $\pi$  quantities, except  $\pi_1$ ,  $\pi_2$ , and  $\pi_3$ , should be expanded into dimensions. Because  $\pi$  quantities are dimensionless numbers, the dimensions of the physical quantities are written in the dimensions of length  $L$ , time  $T$ , and mass  $M$  as follows:

$$\left. \begin{aligned} \dim V &= \dim r^{x_0} \rho^{y_0} g^{z_0} \\ \dim v &= \dim r^{x_4} \rho^{y_4} g^{z_4} \\ \dim B &= \dim r^{x_5} \rho^{y_5} g^{z_5} \\ \dim H &= \dim r^{x_6} \rho^{y_6} g^{z_6} \\ \dim \omega &= \dim r^{x_7} \rho^{y_7} g^{z_7} \\ \dim R_1 &= \dim r^{x_8} \rho^{y_8} g^{z_8} \end{aligned} \right\} \Rightarrow \left. \begin{aligned} LT^{-1} &= L^{x_0-3y_0+z_0} M^{y_0} T^{-2z_0} \\ L^2 T^{-1} &= L^{x_4-3y_4+z_4} M^{y_4} T^{-2z_4} \\ L &= L^{x_5-3y_5+z_5} M^{y_5} T^{-2z_5} \\ L &= L^{x_6-3y_6+z_6} M^{y_6} T^{-2z_6} \\ T^{-1} &= L^{x_7-3y_7+z_7} M^{y_7} T^{-2z_7} \\ L &= L^{x_8-3y_8+z_8} M^{y_8} T^{-2z_8} \end{aligned} \right\} \quad (4)$$

The exponents of each dimension must be the same on both sides of the equations, so the following equations can be obtained:

$$\left. \begin{aligned} \begin{cases} 1 = x_0 - 3y_0 + z_0 \\ 0 = y_0 \\ -1 = -2z_0 \end{cases} &\Rightarrow \begin{cases} x_0 = 1/2 \\ y_0 = 0 \\ z_0 = 1/2 \end{cases} &\Rightarrow \pi = \frac{V}{r^{x_0} \rho^{y_0} g^{z_0}} = \frac{V}{\sqrt{rg}} \\ \begin{cases} 2 = x_4 - 3y_4 + z_4 \\ 0 = y_4 \\ -1 = -2z_4 \end{cases} &\Rightarrow \begin{cases} x_4 = 3/2 \\ y_4 = 0 \\ z_4 = 1/2 \end{cases} &\Rightarrow \pi_4 = \frac{v}{r^{x_4} \rho^{y_4} g^{z_4}} = \frac{v}{r^{3/2} g^{1/2}} \\ \begin{cases} 1 = x_5 - 3y_5 + z_5 \\ 0 = y_5 \\ 0 = -2z_5 \end{cases} &\Rightarrow \begin{cases} x_5 = 1 \\ y_5 = 0 \\ z_5 = 1 \end{cases} &\Rightarrow \pi_5 = \frac{B}{r^{x_5} \rho^{y_5} g^{z_5}} = \frac{B}{r} \\ \begin{cases} 1 = x_6 - 3y_6 + z_6 \\ 0 = y_6 \\ 0 = -2z_6 \end{cases} &\Rightarrow \begin{cases} x_6 = 1 \\ y_6 = 0 \\ z_6 = 0 \end{cases} &\Rightarrow \pi_6 = \frac{H}{r^{x_6} \rho^{y_6} g^{z_6}} = \frac{H}{r} \\ \begin{cases} 0 = x_7 - 3y_7 + z_7 \\ 0 = y_7 \\ -1 = -2z_7 \end{cases} &\Rightarrow \begin{cases} x_7 = -1/2 \\ y_7 = 0 \\ z_7 = 1/2 \end{cases} &\Rightarrow \pi_7 = \frac{\omega}{r^{x_7} \rho^{y_7} g^{z_7}} = \frac{\omega}{r^{-1/2} g^{1/2}} \\ \begin{cases} 1 = x_8 - 3y_8 + z_8 \\ 0 = y_8 \\ 0 = -2z_8 \end{cases} &\Rightarrow \begin{cases} x_8 = 1 \\ y_8 = 0 \\ z_8 = 0 \end{cases} &\Rightarrow \pi_8 = \frac{R_1}{r^{x_8} \rho^{y_8} g^{z_8}} = \frac{R_1}{r} \end{aligned} \right\} \quad (5)$$

Substituting the above  $\pi$  dimensionless numbers of Eq. (5) into the dimensionless governing Eq. (2) yields the following:

$$\frac{V}{\sqrt{rg}} = f\left(\frac{v}{r^{3/2} g^{1/2}}, \frac{B}{r}, \frac{H}{r}, \frac{\omega}{r^{-1/2} g^{1/2}}, \frac{R_1}{r}\right) \quad (6)$$

So,

$$V = \phi \sqrt{rg} \quad (7)$$

where  $\phi$  is a dimensionless number, and  $\phi = f\left(\frac{v}{r^{3/2} g^{1/2}}, \frac{B}{r}, \frac{H}{r}, \frac{\omega}{r^{-1/2} g^{1/2}}, \frac{R_1}{r}\right)$ . Eq. (7) is the relationship

between the average velocity over a cross section ( $V$ ) and the radius size of impellers ( $r$ ), in which the coefficient can be determined by CFD or experiments.

### 3. Simulation and analysis of the variation of average velocity with radius size of impellers

#### 3.1. Governing equations

In most engineering practice, the time-averaged properties of flows are enough to provide the required information, which are obtained by solving the time-averaged equations for the flows in a whole range of turbulent scales to be modeled [19]. Thus, this modeling approach can greatly reduce required computational efforts and resources and is widely adopted for practical engineering applications [19].

The unsteady incompressible time-averaged mass and momentum conservation equations can, respectively, be written as follows [11,14,17, and 19]:

$$\frac{\partial \rho}{\partial t} + \frac{\partial(\rho u_i)}{\partial x_i} = 0 \quad (8)$$

and

$$\begin{aligned} \frac{\partial(\rho u_i)}{\partial t} + \frac{\partial(\rho u_i u_j)}{\partial x_j} \\ = -\frac{\partial p}{\partial x_i} + \frac{\partial}{\partial x_j} \left[ \mu \left( \frac{\partial u_i}{\partial x_j} + \frac{\partial u_j}{\partial x_i} \right) \right] - \frac{\partial}{\partial x_j} (\overline{\rho u_i' u_j'}) + \rho g_i \end{aligned} \quad (9)$$

where  $\rho$  is density;  $t$  is time;  $x_i$  is the space coordinate in  $i$  direction;  $p$  is pressure;  $\mu$  is molecular dynamic viscosity;  $g_i$  is the gravitational acceleration in  $i$  direction;  $u_i$  and  $u_i'$  are the time-averaged and fluctuating velocity components in  $i$  direction, respectively; and the subscripts  $i, j = 1, 2, 3$ .

The Reynolds-averaged N-S equations are always closed by the principal turbulence models, such as the standard  $k-\epsilon$  model, and the relatively improved models named by the RNG and the realizable  $k-\epsilon$  models in popular CFD [17,19].

The term  $-\overline{\rho u_i u_j'}$ , in Eq. (9), is defined as Reynolds stress and must be modeled. In all the two-equation turbulence models, the modeling approach of Reynolds stress always assumes a locally isotropic turbulence and employs the Boussinesq hypothesis relating these stresses to the mean deformation rates and mean velocity gradients [19]:

$$-\overline{\rho u_i u_j'} = \mu_t \left( \frac{\partial u_i}{\partial x_j} + \frac{\partial u_j}{\partial x_i} \right) - \frac{2}{3} \left( \rho k + \mu_t \frac{\partial u_i}{\partial x_i} \right) \delta_{ij} \quad (10)$$

where  $\mu_t$  is the turbulent dynamic viscosity and computed as a function of turbulent kinetic energy  $k$  and kinetic energy dissipation rate  $\epsilon$  [19]:

$$\mu_t = \rho C_\mu \frac{k^2}{\epsilon} \quad (11)$$

where  $C_\mu$  is a model constant with a value of 0.085.

The transport equations for  $k$  and  $\epsilon$  in RNG  $k$ - $\epsilon$  turbulence model are given as follows [19]:

$$\frac{\partial(\rho k)}{\partial t} + \frac{\partial(\rho k u_i)}{\partial x_i} = \frac{\partial}{\partial x_j} \left[ \left( \mu + \frac{\mu_t}{\sigma_k} \right) \frac{\partial k}{\partial x_j} \right] + G_k - \rho \epsilon \quad (12)$$

and

$$\frac{\partial(\rho \epsilon)}{\partial t} + \frac{\partial(\rho \epsilon u_i)}{\partial x_i} = \frac{\partial}{\partial x_j} \left[ \left( \mu + \frac{\mu_t}{\sigma_\epsilon} \right) \frac{\partial \epsilon}{\partial x_j} \right] + C_1^* \frac{\epsilon}{k} G_k - \rho C_2 \frac{\epsilon^2}{k} \quad (13)$$

where  $\sigma_k$ ,  $C_1$ ,  $C_2$ , and  $\sigma_\epsilon$  are empirical constants and have the value of 0.7179, 1.42, 1.68, and 0.7179, respectively; and other parameters are  $C_1^* = C_1 - \eta(1 - \eta/\eta_0)/(1 + \beta\eta^3)$ ,  $\tilde{\eta} = SK/\epsilon$ ,  $S = (2S_{i,j}S_{i,j})^{1/2}$ ,  $\tilde{\eta}_0 = 4.38$ ,  $\beta = 0.015$ , and  $S_{i,j} = (\partial u_i/\partial x_j + \partial u_j/\partial x_i)/2$ .

### 3.2. Calculated model and grid generation

The height of side wall of the Carrousel OD is 5 m. The water depth is 4.5 m. The OD consists of four channels, respectively, named A, B, C, and D with a width of 8.5 m, and three small bends with a radius of 8.5 m, and one big bend with a radius of 17 m. The length of the simulated domain is 109 m, width 34.6 m, and height 6 m. The thickness of the walls is 0.2 m. The capacity of the wastewater treatment is 25,000 m<sup>3</sup>/d. Three impellers are installed at both ends of the OD. In the numerical calculation, the details of the calculation region are shown in Fig. 1 [19].

The computational domain is divided into 172,640 meshes generated by the GAMBIT procedure, which are composed of structural meshes in the straight channels and unstructured meshes in the other part. The maximum mesh size is 2.5 m and the minimum 0.25 m. The 3D meshes and the 2D horizontal plan meshes for the computational domain are shown in Figs. 2(a) and (b).

The numerical validation of the computational mesh independence has been performed to meet the requirement of the simulation. Using the same initial and boundary conditions, the flow fields for the OD with 172,640 meshes and 182,640 meshes are computed, respectively, the comparison of the velocity component in  $x$  direction along the vertical line at a point of  $x = 60$  m and  $y = 4.25$  m shows a good agreement in Fig. 3, and the solid line represents the velocity component in  $x$  direction for the 172,640 meshes and the triangular points for the 182,640 meshes, which validates that the computational grid with 172,640 meshes is an independent one.

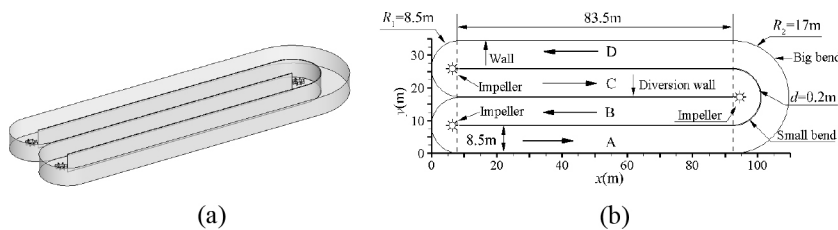


Fig. 1. Computational domain: (a) 3D region and (b) 2D horizontal plan.

The detail description of the impellers is shown in Fig. 4. Fig. 4(a) shows the shape of the impellers; Figs. 4(b) and (c) show the detail dimensions of the impellers: the radius of the impeller's shaft is 0.95 m, the diameter of the impeller is 3.7 m, the length of the blades is 2.95 m, and height 0.75 m; and Fig. 4(d) shows the 3D meshes for the impellers.

### 3.3. Initial and boundary conditions and solution method for the equations

The flow inlet and outlet conditions for an OD have little influence on the flow field, so they were ignored in the numerical calculation [11,14,17]. Water flow in OD has a free water surface, and the water surface is nearly taken as a plane above which there is air. Thus, the water surface is assumed to be flat so that the boundary condition for it could be given by a “rigid-lid” method [19]. The wall function is used for the side walls and bottom as a boundary condition. The stationary water depth is given as the initial condition. The motion of the submerged impellers relative to an OD is described by a multiple reference frame model [19]. The radius size of submerged impellers is specified at 1.25 m, 1.85 m, 2.50 m, 3.12 m, and 3.75 m, respectively.

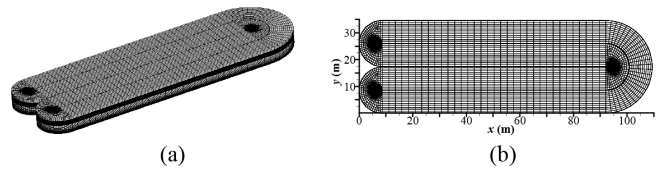


Fig. 2. Grids of the computational domain: (a) 3D grid and (b) 2D horizontal plan grid.

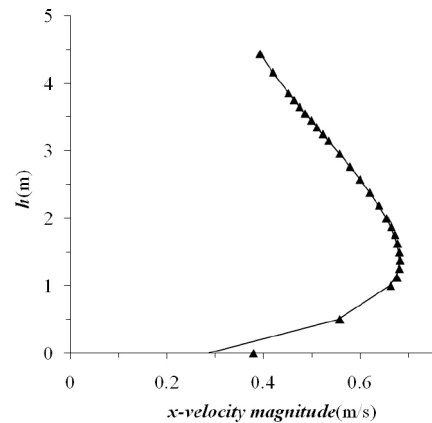


Fig. 3. Comparison of the velocity component in  $x$ -direction along the vertical line at a point of  $x = 60$  m and  $y = 4.25$  m between the two kinds of mesh.

Eqs. (8), (9), (12), and (13) were discretized by the finite volume method, and solved by the pressure implicit with splitting of operators algorithm for the velocity and pressure fields.

3.4. Analysis of the simulated results

3.4.1. Analysis of the flow fields and the variation of average velocity with the radius size of impellers

OD is a structure composed of bend and straight channels (Fig. 1). The smaller average velocity of the flow may

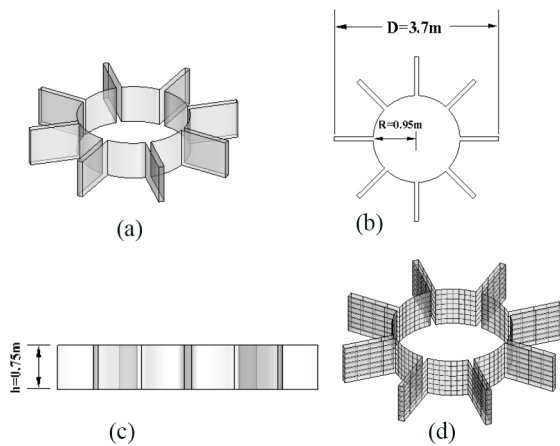


Fig. 4. Detail descriptions of the impellers: (a) 3D shape of the impeller, (b) detail dimensions from top view, (c) detailed dimensions from front view, and (d) 3D meshes for the impellers.

cause sludge phase retention in an OD, which is adverse to its operation [19]. The radius size of impellers has a great effect on the average velocity over a cross section. Here, the average velocity under different radius sizes, 1.25 m, 1.85 m, 2.50 m, 3.12 m, and 3.75 m, of impellers was simulated. The simulated velocity fields and streamlines on the horizontal plane with submerged depth to the total water depth of 0.45 are shown in Fig. 5.

Fig. 5 shows that the flow velocity is larger near the impellers and relatively smaller away from the impellers. When water flows into a straight channel, the recirculation zone is formed at the inner side of the straight channel because of the uneven flow velocity. The flow velocity inside the recirculation zone is smaller and outside is larger. Along the direction of flowing, as the energy loss and the effective cross-section area gradually become larger, the sectional average velocity gradually becomes smaller. When flow passes through the next impeller, owing to the flow added by energy, the velocity becomes larger. The recirculation zone gradually increases with an increasing radius size of impellers, which is mainly because with a constant rotational speed of impellers, the velocity at a point on the impeller blade increases with an increase in the distance from the point to the rotation center. The larger radius of impellers will result in a further uneven velocity distribution at the bend outlets, which leads to a further larger recirculation zone. At the same time, with an increase in the radius size of impellers, the entrainment effect of the surrounding water will be enhanced, which has a great effect on the flow structure of OD. Therefore, it is obtained that a larger radius size of impellers can generate a further uneven velocity distribution so as to form a larger recirculation zone. Therefore, with a constant rotational speed, the radius size

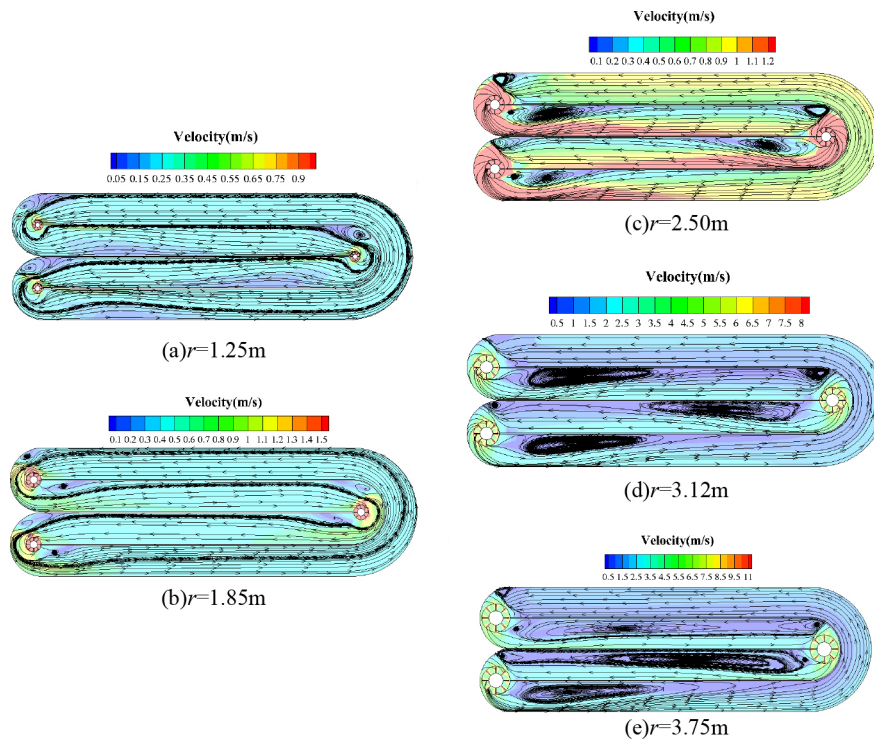


Fig. 5. Simulated velocity fields and streamlines on the horizontal plane for different radii: (a)  $r = 1.25$  m, (b)  $r = 1.85$  m, (c)  $r = 2.50$  m, (d)  $r = 3.12$  m, and (e)  $r = 3.75$  m.

of impellers can be neither too larger nor too smaller. Larger radius will cause larger circulation size, which affects the effective volume of OD; smaller radius will cause sectional average velocity not to meet its requirement so that solid settlement is formed. The sectional average velocity of an OD is not less than 0.3 m/s, which is required for OD design [11].

Here, the simulated average velocities of the flows with different radii of impellers for this OD are shown in Table 1, according to which the fitting line is obtained, as shown in Fig. 6, and the relationship for the variation of  $V$  with  $r$  is given as follows:

$$V = 0.53\sqrt{rg} - 1.754 \tag{14}$$

with  $r$  in the reference range of  $1.25 \leq r \leq 3.75$  m. Eq. (14) shows that the variation of average velocity of flow over a cross section with radius size of impellers is nearly in a linear relationship, according to which the best radius size can be found. We obtain that the minor radius size of 1.53 m can achieve the required minor sectional average velocity of 0.3 m/s for the OD.

3.4.2. Analysis of impeller rotation speed to achieve reference sectional velocity of 0.3 m/s

Liu et al. [19] solved the problem about the influence of rotational speed of impellers with a constant radius size on the cross-sectional average velocity of flow in an OD and obtained an equation describing the cross-sectional average velocity of flow varying with the rotational speed of impellers with a constant radius size, while this research solved the problem about the influence of radius size of impellers with a constant rotational speed on the cross-sectional average velocity of flow in the OD. The two researches used the

Table 1  
Simulated average velocities of the flows with different radii of impellers

Average velocity over a cross-section, $V$ (m/s)	0.19	0.48	0.74	1.10	1.60
Radius of impellers, $r$ (m)	1.25	1.85	2.50	3.12	3.75
$\sqrt{rg}$ (m/s)	3.50	4.26	4.95	5.53	6.06

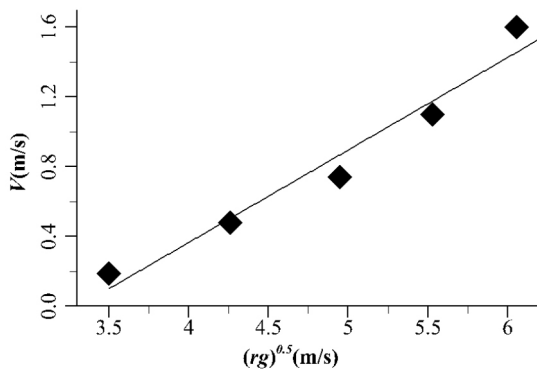


Fig. 6. Variation of  $V$  with  $r$ .

same physical model in solving the two different problems. Liu et al. [19] obtained the equation for the cross-sectional average velocity of flow varying with the rotational speed of impellers with a constant radius size, that is,  $v = -0.485g/\omega + 1.956$ , with  $g/\omega$  in the reference range of  $1.34 < g/\omega < 3.0$ , from which the minor impeller rotational speed, 2.87 (rad/s), can be obtained to achieve the required minor sectional average velocity, 0.3 m/s, for the OD.

3.4.3. Analysis of energy efficiency for each impeller at a fixed flow speed

The energy efficiency for an impeller can defined as follows:

$$P = \gamma QE \tag{15}$$

where  $P$  is energy efficiency for an impeller;  $\gamma$  is specific weight;  $Q$  is water discharge rate; and  $E$  is the energy difference between the inlet and outlet sections of the bend shown in Fig. 7, the express for  $E$  is as follows:

$$E = z_{i+1} + \frac{p_{i+1}}{\gamma} + \frac{\alpha_{i+1}v_{i+1}^2}{2g} - (z_i + \frac{p_i}{\gamma} + \frac{\alpha_i v_i^2}{2g}) \tag{16}$$

where  $z$  represents an elevation above any arbitrary datum plane;  $p$  is the pressure;  $v$  is the sectional average velocity; and  $\alpha$  is an empirical constant with a value of 1.0.

The sectional average velocities and water depths for sections are shown in Table 2, substitution of which into Eq. (16) gives the energy difference between the inlet and outlet sections of the bends shown in Fig. 7, 0.021 m for Impeller 1, 0.012 m for Impeller 2, and 0.011 m for Impeller 3. Using Eq. (1), the energy efficiency for each impeller can be obtained, 3,704.4 W for Impeller 1, 2,116.8 W for Impeller 2, and 1,940.4 W for Impeller 3. As shown in Fig. 7, the lengths of flow path along the flowing direction from Sections 2–5 and 6–3 are almost the same and are about half of that from

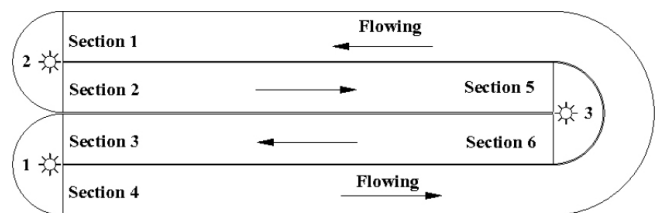


Fig. 7. Sketch for the position of cross-sections.

Table 2  
Sectional average velocity and water depth for each section

Sections	Water depth (m)	Sectional average velocity (m/s)
1	4.545	0.630
2	4.541	0.794
3	4.543	0.606
4	4.526	0.884
5	4.546	0.627
6	4.539	0.779

Sections 4–1, which causes that the water head loss (energy loss) from Sections 4–1 is much bigger than those from Sections 2–5 and 6–3. Therefore, the energy efficiency for Impeller 1 is the biggest, and those for Impellers 2 and 3 are nearly the same, and smaller than that of Impellers 1. The analysis of energy efficiency for each impeller at a fixed flow speed shows that the energy efficiency was much affected by the energy loss of the open-channel flow from the downstream of the impeller to the next impeller.

#### 4. Some discussions and further study plan

With a constant rotational speed of impellers, a larger radius of impellers will result in the average velocity of the flows to be increased. Therefore, according to the OD designing rule that the average fluid-velocity over a cross section is greater than 0.3 m/s is required, the radius size of impellers corresponding to the average velocity of 0.3 m/s should be determined, which will be useful for the efficiency of water treatment [11].

Dimensionless parameters significantly deepen our understanding of fluid-flow phenomena; even can provide some ways to find some laws of physical phenomena. By grouping significant quantities into dimensionless parameters, it is possible to reduce the number of variables and to make this compact result (equations or data plots) applicable to all similar situations [18,19]. Here, dimensional analysis method is used to find that the relationship between the average velocity of the flow and the radius size of impellers in OD. Still, the coefficient of the relationship equation is obtained by the numerical simulation results. The relationship could be applicable for similar ODs. But for the similar ODs, the coefficients in the relationship maybe different, which should be determined by CFD or experiments.

Experiment is the main way to investigate a new basic phenomenon, taking a large amount of observation data as the foundation, still, the validation for a numerical simulation result must use the measured (in prototype or model) data [18,19]. Next, further study will be carried out to validate the simulation result by an experimental method. An experimental model for the actual Carrousel OD will be made of organic glass, according to the gravity similarity law (also named Froude number similarity theory) [18]. The experiment will be performed under the same working conditions used in the above simulations. The measured average velocities of the flows in the model are changed to that of the actual Carrousel OD, and can be used to compare with the simulation results, and further, the reliability of the simulation results will be validated. Then, the CFD method can predict the flow fields in an OD with different radii of impellers, and can be used to determine a proper radius of impellers.

#### 5. Conclusions

In this paper, the dimensional analysis and numerical simulation methods are used to study the relationship between the average velocity of the flow and the radius size of impellers. According to the fitting of the points for the simulated results with different radii of impellers, the equation for the variation of  $V$  with  $r$  can be approximately

written as  $V = 0.53\sqrt{rg} - 1.754$ , with  $r$  in the reference range of  $1.25 \leq r \leq 3.75$  m, which is in agreement with the dimensional analysis result, by which the minor radius size of 1.53 m can achieve the required minor sectional average velocity of 0.3 m/s for the OD. After analysis of the influence of impeller rotation speed, the minor impeller rotational speed of 2.87 rad/s was obtained to achieve the required minor sectional average velocity of 0.3 m/s for the OD. In addition, the analysis of energy efficiency for each impeller at a fixed flow speed shows that the energy efficiency was much affected by the energy loss of the open-channel flow from the downstream of the impeller to the next impeller.

The effect of the radius of impellers on the flow fields was numerically simulated by the experimentally validated mathematical model in the OD. The above results and the research method could be applicable for similar ODs. Next, further study will be carried out to validate the simulation results by an experimental method.

#### Acknowledgments

Financial support for this study was provided by the National Natural Science Foundation of China (Grant No. 51578452 and 51178391) and the scientific research projects of Shaanxi Province (2016GY-180 and 2014K15-03-05).

#### Symbols

$B$	—	Width of the straight channel in OD, m
$C$	—	Model parameter in Eq. (11) with a value of 0.085
$C_1$	—	Model parameter with a value of 1.42 for computing $C_1^*$
$C_1^*$	—	Model parameter in Eq. (13)
$C_2$	—	Model parameter in Eq. (13) with a value of 1.68
$E$	—	Energy difference, m
$g_i$	—	Gravitational acceleration in $i$ direction, $i = 1, 2, 3$ , $m/s^2$
$H$	—	The water depth, m
$k$	—	Turbulent kinetic energy, $m^2/s^2$
$p$	—	Pressure, $kg/m s^2$
$P$	—	Energy efficiency for an impeller, Nm/s or w
$Q$	—	Water discharge rate, $m^3/s$
$G_k$	—	Production term in Eqs. (12) and (13)
$r$	—	Radius of impellers, m
$R_1, R_2$	—	Radius of bends, m
$S$	—	Parameter for computing $C_1^*$
$S_{ij}$	—	Parameter for computing $C_1^*$
$t$	—	Time, s
$u_i$	—	Velocity component in $i$ direction, $i = 1, 2, 3$ , m/s
$u_i'$	—	Fluctuating velocity component in $i$ direction, $i = 1, 2, 3$ , m/s
$V, v$	—	Sectional average velocity, m/s
$x_i$	—	Space coordinate in $i$ direction, $i = 1, 2, 3$ , m
$z$	—	An elevation above any arbitrary datum plane, m
ADV	—	Acoustic Doppler velocimeter
CFD	—	Computational Fluid Dynamics
DO	—	Dissolved oxygen
N-S	—	Navier–Stokes
OD	—	Oxidation ditch
RNG	—	Renormalized group

## Greeks

- $\alpha$  — An empirical constant with a value of 1.0 in Eq. (16)
- $\beta$  — A constant of 0.015 for computing  $C_1^*$
- $\delta_{ij}$  — Kronecker function in Eq. (10),  $\delta_{ij} = 1$  with  $i = j$ , and  $\delta_{ij} = 0$  with  $i \neq j$
- $\varepsilon$  — Kinetic energy dissipation rate,  $\text{m}^2/\text{s}^3$
- $\gamma$  — Specific weight of water,  $\text{N}/\text{m}^3$
- $\eta$  — Parameter for computing  $C_1^*$
- $\tilde{\eta}_0$  — A constant of 4.38 for computing  $C_1^*$
- $\mu$  — Molecular dynamic viscosity,  $\text{kg}/(\text{m} \times \text{s})$
- $\mu_t$  — Turbulent dynamic viscosity,  $\text{kg}/(\text{m} \times \text{s})$
- $\rho$  — Density,  $\text{kg}/\text{m}^3$
- $\sigma_k$  — Model parameter in Eq. (12) with a value of 0.7197
- $\sigma_\varepsilon$  — Model parameter in Eq. (13) with a value of 0.7197
- $\pi$  — Dimensionless number
- $\phi$  — Dimensionless parameter
- $\omega$  — Rotational speed,  $\text{rad}/\text{s}$
- $\nu$  — Kinematic viscosity of water in Eq. (1),  $\text{m}^2/\text{s}$

## Subscripts

- $i, j$  — Direction,  $i = 1, 2, 3; j = 1, 2, 3$
- $t$  — Turbulence

## References

- [1] Y. Yang, J. Yang, J. Zuo, Y. Li, Sh. He, X. Yang, K. Zhang, Study on two operating conditions of a full-scale oxidation ditch for optimization of energy consumption and effluent quality by using CFD model, *Water Res.*, 45 (2011) 3439–3452.
- [2] C.P. Grady, G.T. Daigger, H.C. Lim, *Biological Wastewater Treatment*, Marcel Dekker Inc., New York, 1999.
- [3] V. Diamantis, I. Papaspyrou, P. Melidis, A. Aivasidis, High aeration rate enhances flow stratification in full-scale oxidation ditch, *Bioprocess. Biosyst. Eng.*, 33 (2010) 293–298.
- [4] L. Fan, D. Chen, Y. Liu, Zh. Wang, H. Shi, Model test and comparative analysis of flow in a carousel oxidation ditch with one aerator, *Res. Environ. Sci.*, 20 (2007) 97–101.
- [5] S. Simon, Prediction of mean circulation velocity in oxidation ditch, *Environ. Technol.*, 22 (2001) 195–204.
- [6] D. Xu, D. Zhang, Zh. Chen, Sh. Yang, T. Zhang, Stereoscopic PIV measurement of 3-dimensional flow field in carousel oxidation ditch reactor model, *Chin. J. Appl. Mech.*, 25 (2008) 387–391.
- [7] L. Fan, D. Chen, Zh. Wang, Y. Liu, H. Shi, Study on flow characteristic of Carousel oxidation ditch, *Tech. Equip. Pollut. Control*, 07 (2006) 36–41.
- [8] Q. Liu, J. He, Influence of submerged impellers on oxidation ditch flow characteristics, *Environ. Sci. Technol.*, 35 (2012) 93–98.
- [9] J. Zhao, L. Zhang, L. Liu, D. Cheng, Z. Zhe, M. He, H. Zhou, D. Zhu, Test and analysis on flow pattern of application scale oxidation ditch, *Environ. Pollut. Control*, 32 (2010) 21–24.
- [10] W. Wei, Y. Bai, Y. Liu, Optimization of submerged depth of surface aerators for a carousel oxidation ditch based on large eddy simulation with Smagorinsky model, *Water Sci. Technol.*, 73 (2016) 1608–1618.
- [11] Y. Liu, W. Wei, B. Lv, Research on optimal radius ratio of impellers in an oxidation ditch by using numerical simulation, *Desal. Wat. Treat.*, 52 (2014) 2811–2816.
- [12] L. Luo, W. Li, R. Deng, Z. He, T. Wang, Simulation and analysis on three-dimensional flow field of integrative oxidation ditch, *China Water Wastewater*, 19 (2003) 15–18.
- [13] L. Yang, B. Hu, R. Fan, Numerical simulation of oxidation ditch and improvement methods of structural style, *J. Zhengzhou Univ. (Eng. Sci.)*, 03 (2009) 114–117.
- [14] W. Wei, Z. Zhang, Y. Zheng, Y. Liu, Numerical simulation of additional guiding baffles to improve velocity distribution in an oxidation ditch, *Desal. Wat. Treat.*, 57 (2016) 24257–24266.
- [15] L. Li, J. Ni, Three-dimensional three-phase model for simulation of hydrodynamics, oxygen mass transfer, carbon oxidation, nitrification and denitrification in an oxidation ditch, *Water Res.*, 53 (2014) 200–214.
- [16] X. Guo, X. Zhou, Q. Chen, J. Liu, Flow field and dissolved oxygen distributions in the outer channel of the Orbal oxidation ditch by monitor and CFD simulation, *J. Environ. Sci.*, 25 (2013) 645–651.
- [17] W. Wei, Y. Liu, B. Lv, Numerical simulation of optimal submergence depth of impellers in an oxidation ditch, *Desal. Wat. Treat.*, 57 (2016) 8228–8235.
- [18] E. John Finnemore, B. Joseph Franzini, *Fluid Mechanics with Engineering Applications*, 10th ed., McGraw-Hill companies, Inc., New York, NY, USA, 2002.
- [19] Y. Liu, D. Li, W. Wei, B. Lv, J. Wei, Dimensional analysis and numerical simulation methods for the influence of impellers on the average velocity of flows in an oxidation ditch, *Desal. Wat. Treat.*, 81 (2017) 26–32.